ELSEVIER

Journal of Biomechanics 41 (2008) 797–805

JOURNAL OF BIOMECHANICS

www.elsevier.com/locate/jbiomech
www.JBiomech.com

Finite element simulation of arcuates for astigmatism correction

Elena Lanchares[a], Begoña Calvo[a,*], José A. Cristóbal[b], Manuel Doblaré[a]

[a]*Group of Structural Mechanics and Materials Modelling (GEMM), Aragón Institute of Engineering Research (I3A), University of Zaragoza (Spain), Networking Center on Bioengineering, Biomaterials and Nanomedicine (CIBER-BBN), Aragón Institute of Health (ICS), E-50018 Zaragoza, Spain*
[b]*Department of Ophthalmology, Hospital Clínico Universitario Lozano Blesa, E-50009 Zaragoza, Spain*

Accepted 11 November 2007

Abstract

In order to simulate the corneal incisions used to correct astigmatism, a three-dimensional finite element model was generated from a simplified geometry of the anterior half of the ocular globe. A hyperelastic constitutive behavior was assumed for cornea, limbus and sclera, which are collagenous materials with a fiber structure. Due to the preferred orientations of the collagen fibrils, corneal and limbal tissues were considered anisotropic, whereas the sclera was simplified to an isotropic one assuming that fibrils are randomly disposed. The reference configuration, which includes the initial strain distribution that balances the intraocular pressure, is obtained by an iterative process. Then the incisions are simulated. The final positions of the nodes belonging to the incised meridian and to the perpendicular one are fitted by both radii of curvature, which are used to calculate the optical power. The simulated incisions were those specified by Lindstrom's nomogram [Chu, Y., Hardten, D., Lindquist, T., Lindstrom, R., 2005. Astigmatic keratotomy. Duane's Ophthalmology. Lippincott Williams and Wilkins, Philadelphia] to achieve 1.5, 2.25, 3.0, 4.5 and 6.0 D of astigmatic change, using the next values for the parameters: length of 45°, 60° and 90°, an optical zone of 6 mm, single or paired incisions. The model gives results similar to those in Lindstrom's nomogram [Chu et al., 2005] and can be considered a useful tool to plan and simulate refractive surgery by predicting the outcomes of different sorts of incisions and to optimize the values for the parameters involved: depth, length, position.
© 2007 Elsevier Ltd. All rights reserved.

Keywords: Corneal biomechanics; Finite element method; Anisotropy; Hyperelastic behavior; Refractive surgery simulation

1. Introduction

Astigmatism is a refractive error due to the non-spherical shape of the cornea, that is, the refractive power is not uniform in all meridians. Refractive surgery techniques are used to modify the curvature in order to repair the refractive error of the eye. If the corneal astigmatism is the only refractive defect, it may be corrected by making the cornea as spherical as possible. In order to achieve emmetropia, corneal incisions and cataract surgery are often performed at the same time. According to the optical power to be corrected, different sorts of incisions can be performed: radial, arcuates (>3 D) or limbal relaxing ones (1–3 D).

When curved incisions are made, the incised meridian flattens; therefore, they have to be performed in the most curved meridian in order to be flattened. It also causes the perpendicular meridian to be steepened. This effect is usually named by surgeons as *coupling*. The surgeon plans the surgery according to the relation between the amount the incised meridian flattens and how much its perpendicular steepens, predicting this way the optimal result. The parameters to be decided before surgery (number of incisions, angle, depth, shape, symmetry, optical zone) are compiled, according to the optical power to be corrected, in statistically obtained *nomograms*. Nevertheless, an accurate nomogram to be used as a universal reference to achieve a spherical equivalent and astigmatism correction as expected (Cristobal, 2006) is very complex to be obtained. Moreover, the same surgical technique (same angle, optical zone, etc.) usually leads to different results for different patients. It is therefore necessary to study the parameters involved in nomograms and others like the material properties of the cornea which can be quite different between patients with the same level of pathology,

*Corresponding author. Tel.: +34 976 761912; fax: +34 976 762578.
E-mail address: bcalvo@unizar.es (B. Calvo).

0021-9290/$ - see front matter © 2007 Elsevier Ltd. All rights reserved.
doi:10.1016/j.jbiomech.2007.11.010

to plan a patient-specific surgery that minimizes uncertainty in the results. A biomechanical study before surgery is therefore very convenient to assess quantitatively the effect of each parameter on the optical outcome.

Finite element-based biomechanical models of the eye have been presented only recently as a powerful tool for a better prediction of the effects of radial keratotomy and other refractive surgeries. One of the main problems in this case corresponds to the simulation of the complex behavior of the tissues involved. As other biological tissues, the cornea and limbus are composed of an extracellular matrix, highly moisturized, and collagen fibrils disposed in one (limbus) or two (cornea) preferential orientations (Newton and Meek, 1998). For this reason, these materials present a hyperelastic, incompressible and anisotropic constitutive behavior, strongly dependent on the physiological collagen fibril distribution that therefore should be considered in any model. Most works however have used standard constitutive laws. Vito et al. (1989), for instance, considered a linear elastic, homogeneous and isotropic material. Pinsky and Datye (1991) proposed a linear elastic material with anisotropic behavior caused by the collagen fibrils. Velinsky and Bryant (1992) coupled a structural model of the eye, using a linearly elastic, transversely isotropic finite element formulation, with a full-eye optical model. Bryant and McDonnell (1996) compared different material behaviors: linear elastic transversely isotropic, non-linear isotropic and hyperelastic to simulate the membrane inflating test. Le Tallec et al. (1993) used a viscoelastic isotropic hyperelastic incompressible material to study the deformation of the human eye taking into account fibril and solid matrix behaviors. They used a radial distribution of the collagen fibers, although several authors have demonstrated that the preferred orientations of fiber bundles in the apex of the cornea are vertical and horizontal (Aghamohammadzadeh et al., 2004; Newton and Meek, 1998). Recently, hyperelastic anisotropic models have been proposed by several authors (Pinsky et al., 2005; Alastrué et al., 2006; Pandolfi and Maganiello, 2006). In this work, a mechanical model of the human eye based on that proposed by Alastrué et al. (2006) was used. The Holzapfel and Gasser's (2001) strain-energy density function for soft tissues was considered and implemented into a finite element context.

The aim of this study is to obtain a numerical model of the eye capable of estimating the effect on the success of the surgery of the different parameters involved in refractive surgery, trying to get results similar to real ones. Several simulations were performed of a serial of arcuates for the correction of astigmatism. The obtained results were compared to the widely used Lindstrom's nomogram (Chu et al., 2005) (Fig. 1) in order to validate the model.

2. Material and methods

2.1. Finite element model

A three-dimensional finite element model was generated for the anterior half ocular globe geometry (Fig. 2). The ocular globe and the cornea are not exactly sphere-shaped. The real curvature of the cornea lies on a part of an ellipsoid which is a non-revolution volume with different ellipsoidal parameters in each coordinate plane. Nevertheless, a revolution symmetry was assumed for the model to simplify the complexity of the real geometry, assumption widely used by other authors (Alastrué et al., 2006; Pinsky et al., 2005).

Our model is composed of three different parts: cornea, limbus and sclera. The geometric parameters of each part were as follows:

- *Cornea*: external radius 7.5 mm (Cabrera Fernández et al., 2006), corneal thickness 550 μm in the apex and 650 μm in the limbal border (Pinsky and Datye, 1991) and corneal base diameter of 12 mm (Bryant and McDonnell, 1996).
- *Limbus*: ring with internal and external diameters of 12–12.5 mm, respectively, varying thickness from 0.65 mm (corneal border) to 1 mm (scleral border).
- *Sclera*: uniform thickness of 1 mm, external radius of 13 mm.

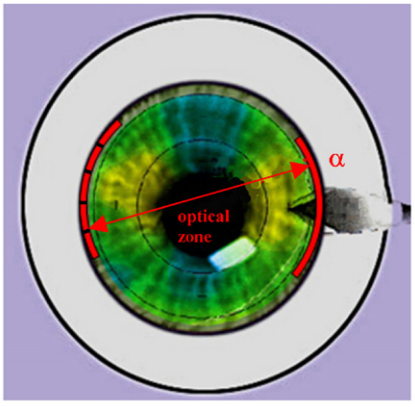

Optical zone (mm)	Nº of incisions	α = 45º	α = 60º	α = 90º
7	1	1.0 D	1.50 D	2.0 D
7	2	2.0 D	3.00 D	4.0 D
6	1	1.5 D	2.25 D	3.0 D
6	2	3.0 D	4.50 D	6.0 D

Fig. 1. Lindstrom's nomogram (Chu et al., 2005).

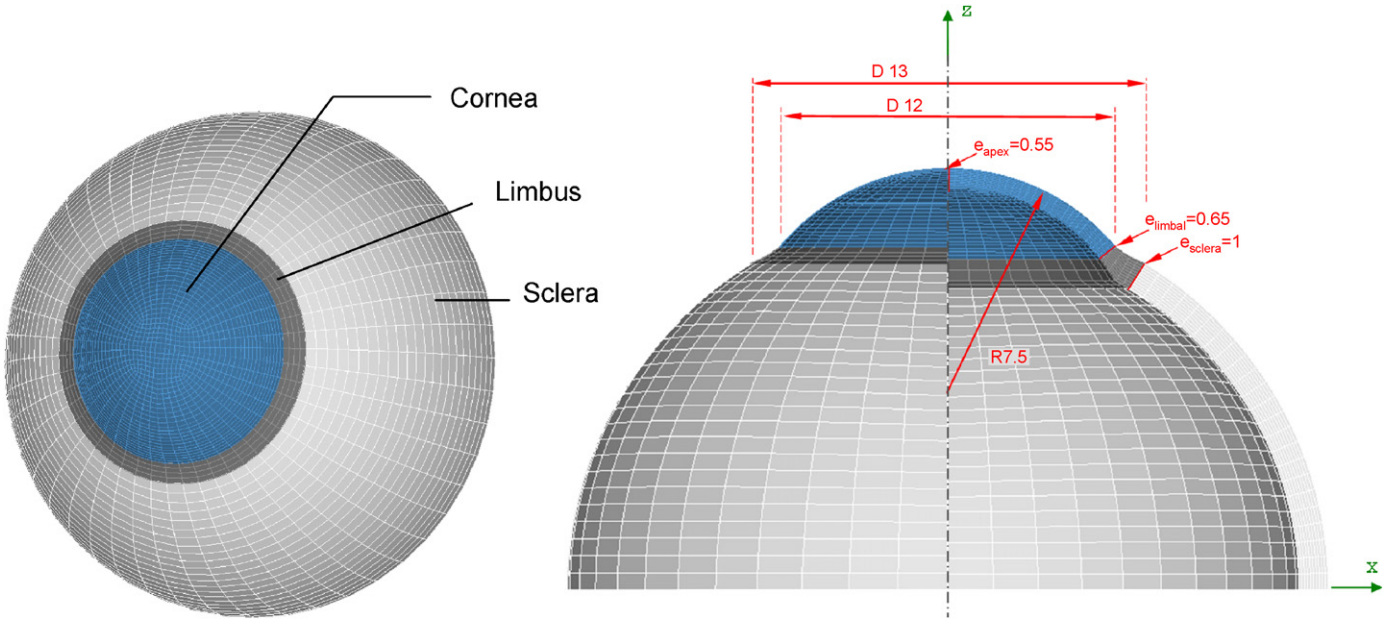

Fig. 2. Model geometry (mm).

Cubit 10.1 (2006) and I-DEAS v.9 (2001) were used to create the geometry and to mesh the model. The mesh was composed of 12.928 hexahedral elements and 27.604 nodes, and was created following a radial pattern (16 segments of 5.625°) to achieve approximately the desired angles to be simulated: 90°, 60° and 45°.

The model was constrained by the following boundary conditions. The displacements of the nodes belonging to the medium plane of the ocular globe in cylindrical coordinates were restrained in tangential and axial directions. Only radial displacements were allowed.

The nodes placed along the optical axis, which includes the apex, were allowed to move only along this direction (*Z*-axis in Fig. 2) while introducing the intraocular pressure (IOP), in order to preserve the symmetry of the model before simulating the incisions.

The inner surface of the modeled ocular globe is subjected to the IOP. This pressure varies from patient to patient and is also influenced by other conditions like age and even the moment of the day. In this work, a value of 15 mm Hg, highly accepted by different authors (Pinsky and Datye, 1991; Shin et al., 1997; Bryant and McDonnell, 1996; Hoeltzel et al., 1992) was used.

2.2. Constitutive model

The living human cornea is highly porous and filled with biological fluid. Approximately 80% of the weight of the cornea is water. It is divided into five layers parallel to its surface. From outside to inside they are: the epithelium, Bowman's membrane, stroma or substantia propia, Descemet's membrane and the endothelium (Pinsky and Datye, 1991). The stroma forms about 90% of the thickness and is divided into 300–500 sheets of collagenous material, the stromal lamellae, parallely distributed to the corneal surface. Lamellae appear to run uninterruptedly from limbus to limbus. Each lamella is about 2–3 mm wide and about 1.5–2.5 μm thick, and does not seem to be interwoven. It is composed of long collagen fibrils embedded in a ground substance, mainly formed of proteoglycans and water. Collagen fibrils lie parallel and run along the whole length of the lamella.

In the central region of the cornea, fibrils are disposed predominantly along the superior–inferior and nasal–temporal directions while near the limbus, they follow the circumferential direction to form a pseudo-annulus. Moreover, there are other randomly oriented fibrils throughout the cornea. This microstructure and the different distributions of collagen fibrils imply an anisotropic behavior for the cornea (Aghamohammadzadeh et al., 2004; Newton and Meek, 1998). In this work, the cornea is considered as an anisotropic material through the definition of two preferred material directions in terms of two local vectors defined at each nodal point. Two fibril directions were defined: one family along the nasal–temporal direction and another along the superior–inferior direction (see Fig. 3). As other authors (Pandolfi and Maganiello, 2006; Pinsky et al., 2005), the circumferential direction of collagen fibrils in the periphery of the cornea was modelled by taking the limbus as a material similar to cornea with only one preferred direction.

Usually, the description of the constitutive behavior of this type of material relies on the identification of an appropriate strain-energy density function from which stress–strain relations and local elasticity tensors are derived (Weiss et al., 1996; Pioletti et al., 1998). As other authors (Pena et al. (2005) for ligaments, Holzapfel et al. (2000) for arteries, and Alastrué et al. (2006) and Pinsky and Datye (1991) for cornea), we postulate the existence of a unique decoupled representation of the strain-energy density function Ψ (Simo and Taylor, 1985) to characterize isothermal processes. Because of the directional dependence on the deformation, we require that the function Ψ explicitly depends on both the right Cauchy–Green tensor $\mathbf{C}=\mathbf{F}^{\mathrm{T}}\mathbf{F}$, where $\mathbf{F}$ is the deformation gradient tensor, and the fibers direction $\mathbf{m}_0$ and $\mathbf{n}_0$ in the reference configuration. Since the sign of $\mathbf{m}_0$ and $\mathbf{n}_0$ is not significant, $\boldsymbol{\Psi}$ must be an even function of $\mathbf{m}_0$ and $\mathbf{n}_0$ and so it may be expressed as $\boldsymbol{\Psi}=\boldsymbol{\Psi}(\mathbf{C},\mathbf{M},\mathbf{N})$ where $\mathbf{M}=\mathbf{m}_0\otimes\mathbf{m}_0$ and $\mathbf{N}=\mathbf{n}_0\otimes\mathbf{n}_0$ are structural tensors (Weiss et al., 1996). Based on the volumetric kinematic constrain, the free energy can be written in decoupled form as (Flory, 1961)

$$\Psi(\mathbf{C})=\Psi_{\mathrm{vol}}(J)+\bar{\Psi}(\bar{\mathbf{C}},\mathbf{M},\mathbf{N}), \tag{1}$$

where $\Psi_{\mathrm{vol}}(J)$ describes the change in volume (volumetric) and $\bar{\Psi}(\bar{\mathbf{C}},\mathbf{M},\mathbf{N})$ the change in shape (isochoric) responses of the material. Both are given scalar-valued functions of $J=\det\mathbf{F}$, $\bar{\mathbf{C}}=\bar{\mathbf{F}}^{\mathrm{T}}\bar{\mathbf{F}}$, where $\bar{\mathbf{F}}=J^{-1/3}\mathbf{F}$, $\mathbf{m}_0$ and $\mathbf{n}_0$ (Holzapfel, 2000). In terms of the strain invariants (Spencer, 1954) Ψ can be written as

$$\begin{aligned}\Psi=\Psi_{\mathrm{vol}}(J)+\bar{\Psi}(&\bar{I}_1(\mathbf{C}),\bar{I}_2(\bar{\mathbf{C}}),\bar{I}_4(\bar{\mathbf{C}},m_0),\bar{I}_5(\bar{\mathbf{C}},m_0),\\&\bar{I}_6(\bar{\mathbf{C}},n_0),\bar{I}_7(\bar{\mathbf{C}},n_0),\bar{I}_8(\bar{\mathbf{C}},\mathbf{m}_0,\mathbf{n}_0),\bar{I}_9(\mathbf{m}_0,\mathbf{n}_0)),\end{aligned} \tag{2}$$

where $\bar{I}_1$ and $\bar{I}_2$ are the first two modified strain invariants of the symmetric modified right Cauchy–Green tensor $\bar{\mathbf{C}}$ (note that $\bar{I}_3=1$). The pseudo-invariants $\bar{I}_4,\ldots,\bar{I}_9$ characterize the constitutive response of

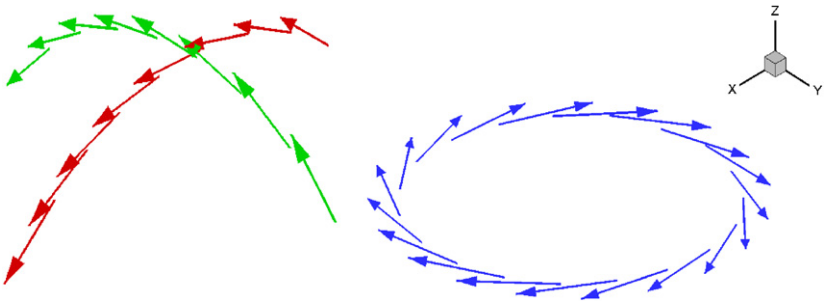

Fig. 3. Directions of the collagen fibrils. Left: cornea $\mathbf{m}_0$ (red), $\mathbf{n}_0$ (green). Right: limbus $\mathbf{n}_0$ (blue).

the fibers (Spencer, 1954). While the invariant $\bar{I}_4$ and $\bar{I}_6$ have a clear physical meaning, the square of the stretch λ along the fiber directions, the influence of $\bar{I}_5$, $\bar{I}_7$ and $\bar{I}_8$ is difficult to evaluate due to the high correlation among the invariants. For this reason and the lack of sufficient experimental data, it is usual not to include these invariants in the definition of Ψ (Weiss et al., 1996). Finally, $\bar{I}_9$ does not depend on the deformation and therefore is not relevant to the constitutive behavior. For a more detailed derivation of the material and space elasticity tensors for completely incompressible or compressible fibered hyperelastic materials and their explicit expressions, see Pérez del Palomar and Doblaré (2006).

For the purposes of this model, the elastic response of the tissue is assumed to arise from the resistance of the collagen fibrils and the matrix, that is, from a unique strain-energy function defined as in Eq. (1). Following other authors (Gardiner and Weiss, 2003), we consider

$$\Psi_{\text{vol}} = \frac{1}{D}(\ln J)^2, \tag{3}$$

which quasi-enforces the null volumetric change depending on the value of the penalty coefficient $1/D$. We use a strain-energy function that combines a Mooney–Rivlin's (Pandolfi and Maganiello, 2006) model to treat the isotropic part corresponding to the matrix behavior and the Holzapfel's model (Holzapfel, 2000) to take into account the anisotropic response of the tissue due to the collagen fibers.

$$\begin{aligned}\Psi_{\text{iso}} &= \Psi_{\text{iso}}^{\text{matrix}} + \Psi_{\text{iso}}^{\text{fibrils}} \\ &= \frac{C_1}{2}(\bar{I}_1 - 3) + \frac{C_2}{2}(\bar{I}_2 - 3) \\ &\quad + \frac{k_1}{2k_2}\{\exp[k_2(\bar{I}_4 - 1)^2] - 1\} + \frac{k_3}{2k_4}\{\exp[k_4(\bar{I}_6 - 1)^2] - 1\}.\end{aligned} \tag{4}$$

To obtain the material constants for the cornea, a non-linear regression method (Holzapfel and Gasser, 2001) was employed using Hoeltzel's experimental stress vs strain curve (Hoeltzel et al., 1992). Since k_1, k_2 represent one direction of fibrils and k_3, k_4 the other, they were assigned the same values in order to model equally all the fibrils, regardless of the orientation. The values for the sclera parameters were adjusted iteratively due to the lack of data in literature (Buzard, 1992). The material constants for cornea (Hoeltzel et al., 1992; Holzapfel and Gasser, 2001), limbus and sclera used in this work are shown in Table 1.

Table 1
Material parameters for cornea, limbus and sclera

Material	C_1 (MPa)	D (MPa^{-1})	C_2 (MPa)	k_1 (MPa)	k_2	K_3 (MPa)	k_4
Cornea	0.1	1e-5	0.0	0.234	29.917	0.234	29.917
Limbus	0.1	1e-5	0.0	0.234	29.917	0	0
Sclera	35	1e-5	−32	0	0	0	0

2.3. Surgery simulation

The curved incisions are cuts performed in the clear cornea, about 90% of the thickness deep and perpendicular to the surface. According to the diopters to be corrected, the parameters of the incisions are chosen: optical zone, length, number of incisions (Fig. 1). After the surgery, the incised meridian flattens, i.e., the corresponding curvature increases, while the meridian orthogonal to the incised one steeps, i.e., the corresponding curvature reduces (Fig. 4). These changes achieve compensation in the refractive difference between the two astigmatic meridians of the cornea.

Before carrying out the simulation, the model has to be driven to a situation that represents the real physiological conditions (Pena et al., 2006). The stress-free configuration of the cornea is not known a priori, only the one deformed by the IOP (Pinsky et al., 2005; Pandolfi and Maganiello, 2006). The point is therefore to introduce in the model the initial strains caused by the IOP, so they have to be calculated in an iterative process.

A user-material subroutine in ABAQUS v6.5 (Hobbit, Karlsson and Sorensen, Inc., 1999) was used to introduce the constitutive behavior and the initial strains into the finite element model. Since the unloaded configuration is unknown, we followed an iterative process to approximately determine the initial strain distribution that balances the IOP in the reference geometry.

The procedure is shown in Fig. 5. The reference configuration Ω_0 is initially stress-free, so the corresponding deformation gradient is $\mathbf{F}_0^0 = \mathbf{I}$. Then IOP is applied on the inner surface of the ocular globe. A new deformed configuration Ω_1 is obtained as the stress distribution balances the externally applied forces. $\mathbf{F}_0^1$ is the corresponding deformation gradient. In the next step, the IOP and $\mathbf{F}_0^1$ are the inputs applied again on Ω_0 and a new configuration Ω_2 corresponding to $\mathbf{F}_0^2$ results. This iterative process is repeated until the deformed configuration is such that the displacements of the nodes in the optical zone are very small and can be considered null (Fig. 6). At this point, the initial strains correspond to the deformation gradient $\mathbf{F}_0^n = \mathbf{F}_{n-1}^n \mathbf{F}_0^{n-1}$.

Once the reference configuration is achieved by balancing the IOP and the initial strains, the next step is the simulation of the incisions. In order to reproduce the incisions with the established parameters such as optical zone, length, depth and shape, the meshing of the model was designed by placing nodes and surfaces between elements exactly where the incision had to be performed. The nodes belonging to these surfaces were initially duplicated but linked by a rough contact. The IOP was then applied to the model using the deformation gradient tensor obtained in the last iteration, $\mathbf{F}_0^n$, and the associated residual stresses as input. The contact between nodes placed at the surfaces where arcuates had to be made was then removed. The incisions of Lindstrom's nomogram (Chu et al., 2005) were simulated for an optical zone of 6 mm and 90% depth (Fig. 7).

3. Results

3.1. Optical power

After surgery simulation, the optical power, measured in diopters, was estimated. The incised astigmatic principal meridian and the secondary one, defined by the final

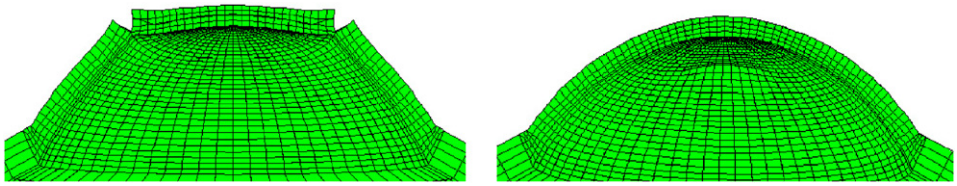

Fig. 4. Flattening and steepening effects. Amplified 10%.

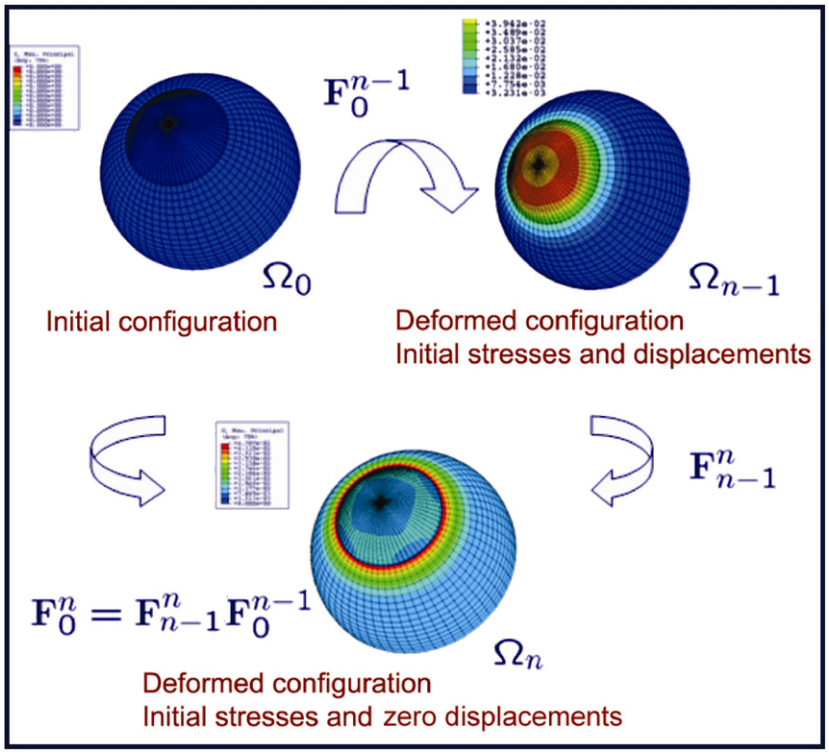

Fig. 5. Iterative process to introduce internal stresses into the initial configuration.

position of the nodes belonging to the corneal anterior surface and inside the optical zone was fitted by means of least squares (Fig. 8). Two radii of curvature were obtained, one for each meridian. Then the diopters were calculated using the expression (Munnerlyn et al., 1988)

$$D \cong \frac{n-1}{R}, \tag{5}$$

where n is the corneal refractive index, whose value is 1.377 and $R[m]$ is the radius of curvature along each meridian (incised and non-incised).

As the optical power depends on the interpolation zone, this influence was studied by varying the radius of the interpolation area from 1.5 mm, minimum fitting optical zone in keratometric maps, and 3 mm, where arcuates were performed. As shown in Table 2, the outcome depends significantly on the fitting optical zone. For the simulation of two incisions, 90° length, a difference of 6% (0.36 D) was obtained between 1.5 and 3 mm of fitting radius. The larger the optical zone, the more similar are the results of the model to the Lindstrom's nomogram (Chu et al., 2005). Therefore, a fitting radius of 3 mm was used for the final analysis.

The estimated optical power in diopters for the simulated incisions is shown in Table 3. All the incisions were performed 3 mm from the apex and a fitting radius of 3 mm was used. The results are very close to those shown in the Lindstrom's nomogram (Chu et al., 2005).

In order to evaluate the influence of the mechanical properties of the tissue on the corneal refractive power after surgery, the simulation was also carried out by varying the values of the constants k_1 and k_2 in expression (4). Although it is not the purpose of this work to perform an extensive sensitivity analysis, it is worth mentioning the slight influence of the constant k_2, for which a 100% change leads to a change of 1% in diopters. In contrast, a 100% change in k_1 leads to a 23.5% change in diopters. To determine the influence of the material properties and others like geometrical ones (anterior and posterior curvatures of the astigmatic axes, corneal thickness) a

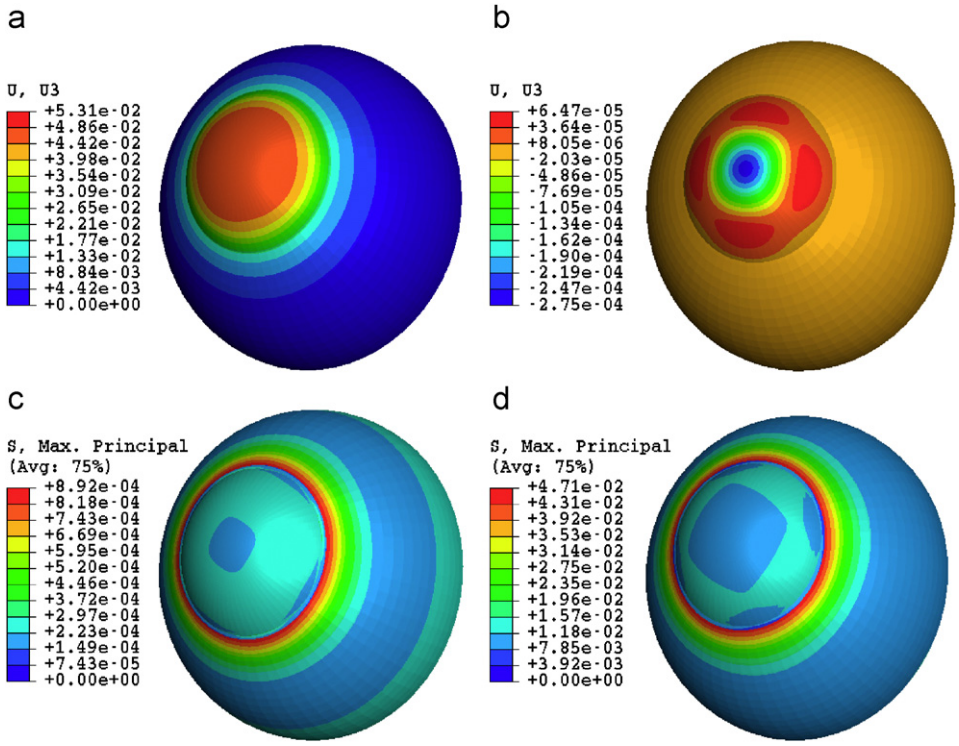

Fig. 6. (a) and (b) Displacements (mm). The maximum displacement at the first iteration is two orders higher than the maximum at the last one. Stress distribution (MPa) in the unloaded (c) and under IOP (d) reference configuration.

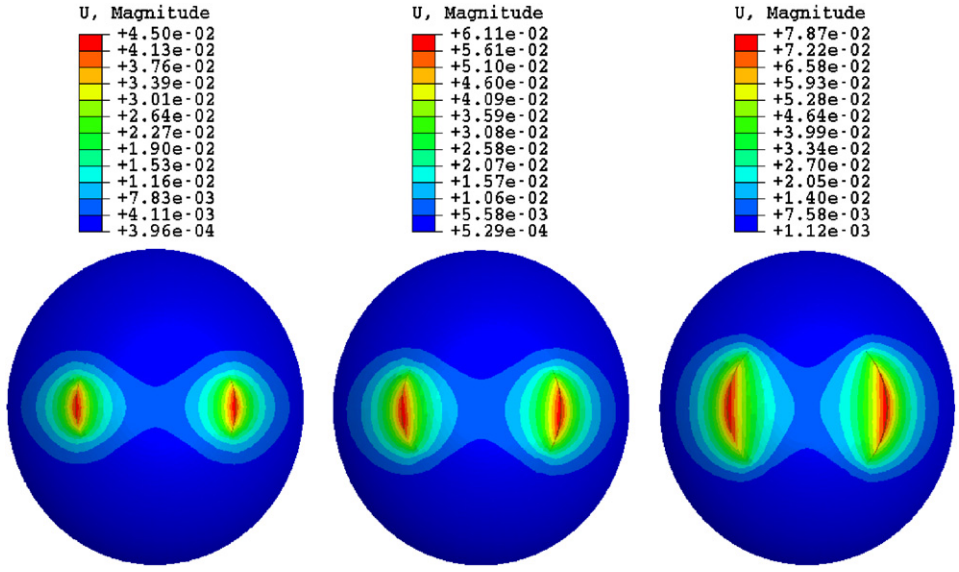

Fig. 7. Cornea after surgery simulation. Incisions 90% depth. 45° (left); 60° (center); 90° (right). Displacements (mm).

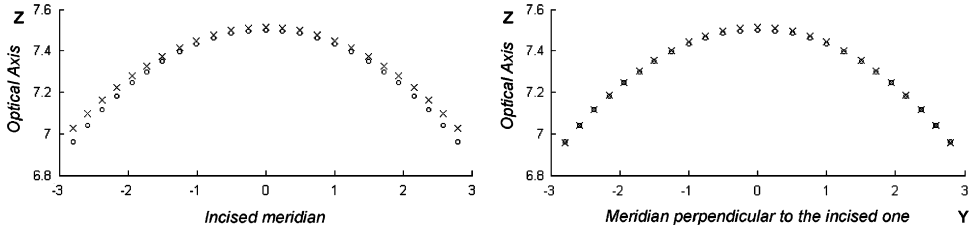

Fig. 8. Nodes of the anterior surface along the incised (left) and non-incised (right) meridians before (○) and after (×) surgery. The vertical axis represents the z-position (along the optical axis). The curves are fitted by least squares to obtain the curvature. Radius of the interpolation area (X-axis): 3 mm.

sensitivity analysis on each parameter involved should be the objective of a future work.

3.2. Stress and strain

The model offers another point of view to analyze the surgery technique and its results. The after-surgical stresses show interesting values and distributions that deserve to be discussed.

In Fig. 9, the maximum principal stress distribution is shown for incisions of 45°, 60° and 90° length. It is obvious that the longer the cut, the higher the gradient of stresses in the cornea.

An example of the usefulness of this model is presented next. To achieve an astigmatic change of 3 D, according to the Lindstrom's nomogram (Chu et al., 2005) paired incisions of 45° length or a single one of 90° length are equally recommended. In Fig. 10, the maximum principal stress and strain distribution for each of these two cases are shown.

In the 90° incision case, the maximum value for the maximum principal stress resulted 4.64×10^{-2} MPa, 30% higher than the maximum value for two 45° incisions. This means that the material suffers a higher damage and consequently would take more time to heal.

On the other hand, it is interesting to observe the contour map obtained for the maximum principal strains. The surgeon would surely choose the paired 45° length incision surgery technique because this way the after-surgical keratometry all over the cornea will be more uniform than in the single 90° length technique. It seems to be a relation between the strain distribution and the keratometric map. Fig. 10(b) shows distributions more or less concentric to the lips of the cuts, for both cases (paired of 45° length and single of 90° length).

Table 2
Influence of the fitting area in surgery induced astigmatism for two arcuates of 90° length

Radius (mm)	1.5	2	2.5	3
D_I	46.6742	46.3530	45.9839	45.6027
D_{NI}	52.2665	52.0702	51.8242	51.5580
D	5.5923	5.7172	5.8403	5.9553

Table 3
Results obtained by simulation, compared to Lindstrom's nomogram for a fitting area of 3 mm radius

No. of incisions	1	1	2	1	2	1
Angle (°)	45	60	45	90	60	90
D Sim. result	1.47	2.13	3	2.72	4.5	5.95
D Lindstrom	1.5	2.25	3	3	4.5	6

4. Discussion

A tool has been developed to simulate incisions for astigmatism correction in order to provide the surgeon a technical evidence to make his decision while planning the surgery or designing new incisional techniques. We present a model composed of cornea, limbus and sclera taking into account the preferred directions of the collagen fibers in each tissue (Pandolfi and Maganiello, 2006). The real *in vivo* conditions of the eye before the surgery simulation were reproduced by introducing the initial strains. The most important aspect of this method is that it does not require previous knowledge of the stress-free configuration, as standard hyperelastic formulations demand. The stress-free geometry is not known *in vivo*, so it is necessary to set

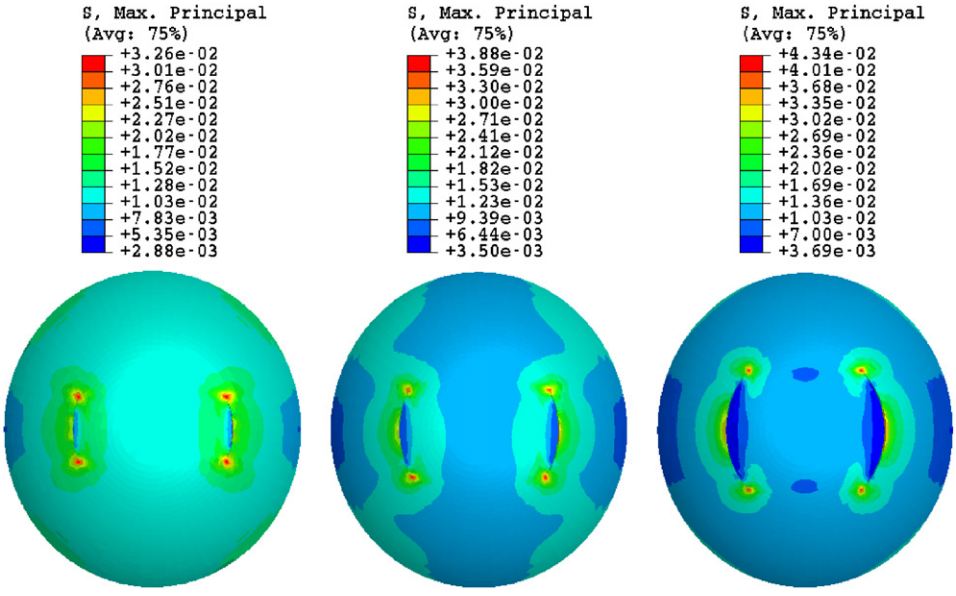

Fig. 9. Maximum principal stresses (MPa). Incisions 90% depth. 45° (left); 60° (center); 90° (right).

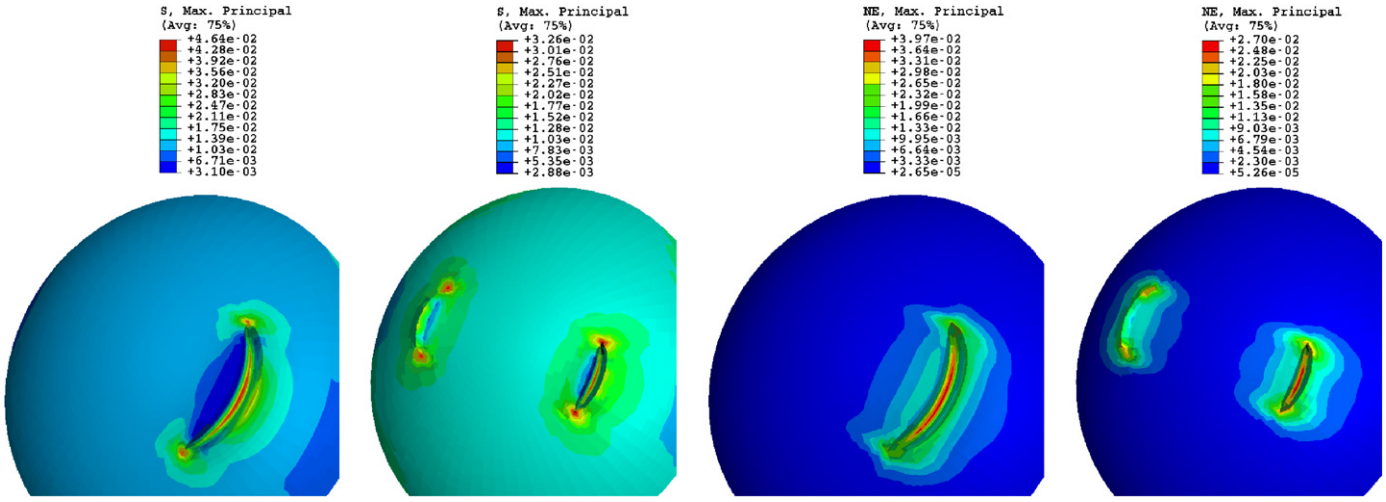

Fig. 10. Maximum principal stresses (left) and strains (right) comparing two cases: one incision, 90° and two incisions, 45°, 90% depth. Amplified 10%.

the model into physiological conditions starting from the deformed geometry and introducing directly the initial strains field. Therefore, the model can be customized to a patient-specific geometry, being not necessary to know the undeformed geometry for each patient.

The results obtained by simulation are similar to those stated in the Lindstrom's nomogram (Chu et al., 2005); therefore, the model is considered suitable for the simulation of refractive surgery at least as a first approach.

The optical power after simulation has been calculated with a very simple expression and it is important to improve this process using optical methods, capable of analyzing the whole optical zone and taking into account not only the anterior surface of the cornea but also the posterior one, therefore providing a value for the diopters more accurate than that obtained individually for the astigmatic meridians (incised and non-incised) of the anterior surface.

It is important to state that the simulation has been made on a healthy sphere-shaped cornea, that is to say, the optical power is 0 D. As clinical evidence shows, the surgically induced astigmatic change does not strongly depend on the astigmatic value before incisional surgery. Therefore, it was assumed that the model's behavior is similar to a real eye and thus the astigmatic change due to the simulated incisions would not be significantly affected by the previous curvature of the meridians. So the results can be understood as incremental ones, supposing that one cornea with that initial value of astigmatism would change with surgery in the same range as it has been simulated, reaching the proposed outcome. This model is only the first step to achieve a future model closer to real geometry, even a patient-specific one.

The model also can be useful for making decisions in surgical planning, taking into account the results of strain distributions. They are not included in nomograms but provide relevant information on the damage of the corneal tissue due to the incisions, which is directly related to the cicatrization period.

Finally, it should be noted the importance of choosing correct values for the material properties. As the clinical evidence shows, the same incisions achieve different optical outcomes for different patients and thus it would be necessary to check if the corneal material properties variation from patient to patient is so relevant to cause these results. The correct values for the material parameters should be obtained by reproducing tests where all the constants were activated, but it is not possible actually to prove whether the range of the proposed values have a physiological validity. As other authors say (Pandolfi and Maganiello, 2006), the validity of material properties requires further experimental investigations than literature reports.

Conflict of interest statement

There is no conflict of interest in this manuscript.

Acknowledgments

The authors gratefully acknowledge the research support of the Spanish Ministry of Education and Science through the research project FIS2005-05020-C03-03.

References

Aghamohammadzadeh, H., Newton, R.H., Meek, K.M., 2004. X-ray scattering used to map the preferred collagen orientation in the human cornea and limbus. Structure 12, 249–256.

Alastrué, V., Calvo, B., Peña, E., Doblaré, M., 2006. Biomechanical modelling of refractive corneal surgery. Journal of Biomechanical Engineering ASME 128 (1), 150–160.

Bryant, M., McDonnell, P., 1996. Constitutive laws for biomechanical modeling of refractive surgery. Journal of Biomechanical Engineering 118, 473–481.

Buzard, K.A., 1992. Introduction to biomechanics of the cornea. Refractive Corneal Surgery 8, 127–138.

Cabrera Fernández, D., Niazy, A., Kurtz, R., Djotyan, G., Juhasz, T., 2006. A finite element model for ultrafast laser-lamellar keratoplasty. Annals of Biomedical Engineering 34, 169–183.

Chu, Y., Hardten, D., Lindquist, T., Lindstrom, R., 2005. Astigmatic keratotomy. Duane's Ophthalmology. Lippincott Williams and Wilkins, Philadelphia.

Computational Modeling Sciences Department, 2006. Sandia National Laboratories. Cubit 10.1 User Documentation. 〈http://cubit.sandia.gov/help-version10.1/cubithelp.htm〉.

Cristobal, J.A., 2006. Corrección del Astigmatismo. Secoir, Madrid.

Flory, P.J., 1961. Thermodynamic relations for high elastic materials. Transaction of the Faraday Society 57, 829–838.

Gardiner, J., Weiss, J., 2003. Subject-specific finite element analysis of the human medial collateral ligament during valgus knee loading. Journal of Orthopaedic Research 21, 1098–1106.

Hobbit, Karlsson and Sorensen, Inc., 1999. Abaqus User's Guide, vol. 5.8. HKS Inc. Pawtucket, RI, USA.

Hoeltzel, D., Altman, P., Buzard, D., Choe, K., 1992. Strip extensometry for comparison of the mechanical response of bovine, rabbit and human corneas. Journal of Biomechanical Engineering 114, 202–215.

Holzapfel, G.A., 2000. Nonlinear Solid Mechanics. Wiley, Chichester.

Holzapfel, G.A., Gasser, T., 2001. A viscoelastic model for fibre-reinforced composites at finite strains: continuum basis, computational aspects and applications. Computer Methods in Applied Mechanics and Engineering 190, 4379–4403.

Holzapfel, G.A., Gasser, T.C., Ogden, R.W., 2000. A new constitutive framework for arterial wall mechanics and a comparative study of material models. Journal of Elasticity 61, 1–48.

Munnerlyn, C., Koons, S.J., Marshall, J., 1988. Photorefractive keratectomy: a technique for laser refractive surgery. Journal of Cataract and Refractive Surgery 14, 46–52.

Newton, R.H., Meek, K.M., 1998. The integration of the corneal and limbal fibrils in the human eye. Biophysical Journal 75, 2508–2512.

Pandolfi, A., Maganiello, F., 2006. A model for the human cornea: constitutive formulation and numerical analysis. Biomechanics and Modelling in Mechanobiology 5, 237–246.

Pena, E., Calvo, B., Martinez, M., Doblaré, M., 2005. A three-dimensional finite element analysis of the combined behavior of ligaments and menisci in the healthy human knee joint. Journal of Biomechanics 39 (9), 1686–1701.

Pena, E., Martinez, M.A., Calvo, B., Doblaré, M., 2006. On the numerical treatment of initial strains in biological soft tissues. International Journal for Numerical Methods in Engineering 68 (8), 836–860.

Pérez del Palomar, A., Doblaré, M., 2006. On the numerical simulation of the mechanical behaviour of articular cartilage. International Journal for Numerical Methods in Engineering 67, 1244–1271.

Pinsky, P., Datye, V., 1991. A microstructurally-based finite element model of the incised human cornea. Journal of Biomedical Engineering 10, 907–922.

Pinsky, P., Heide, D.V.D., Chernyak, D., 2005. Computational modeling of mechanical anisotropy in the cornea and sclera. Journal of Cataract and Refractive Surgery 31, 136–145.

Pioletti, D., Rakotomanana, L., Benvenuti, J.F., Leyvraz, P.F., 1998. Viscoelastic constitutive law in large deformations: application to human knee ligaments and tendons. Journal of Biomechanics 31, 753–757.

Shin, T., Vito, R., Johnson, L., McCarey, B., 1997. The distribution of the strain in the human cornea. Journal of Biomechanics 30, 497–503.

Simo, J.C., Taylor, R.L., 1985. Consistent tangent operators for rate-independent elastoplasticity. Computer Methods in Applied Mechanics and Engineering 48, 101–118.

Spencer, A.J.M., 1954. Theory of Invariants. Continuum Physics. Academic Press, New York.

Structural Dynamics Research Corporation, 2001. I-Deas Tutorials. EDS.

Le Tallec, P., Rahier, C., Kaiss, A., 1993. Three-dimensional incompressible viscoelasticity in large strains: formulation and numerical approximation. Computer Methods in Applied Mechanics and Engineering 109, 233–258.

Velinsky, S., Bryant, M., 1992. On the computer-aided and optimal design of keratorefractive surgery. Refractive Corneal Surgery 8, 173–183.

Vito, R.P., Shin, T.J., McCarey, B.E., 1989. A mechanical model of the cornea: the effects of physiological and surgical factors on radial keratotomy surgery. Refractive Corneal Surgery 5 (2), 82–88.

Weiss, J., Maker, B., Govindjee, S., 1996. Finite element implementation of incompressible, transversely isotropic hyperelasticity. Computer Methods in Applied Mechanics and Engineering 135, 107–128.